Green Chemistry

PAPER

View Article Online
View Journal | View Issue

Cite this: *Green Chem.*, 2024, **26**, 4544

Catalytic self-transfer hydrogenolysis of lignin over Ni/C catalysts†

Xuelei Mei,[a,b] Huizhen Liu, *[c,d] Haihong Wu, *[a,b] Wei Wu,[a,b] Bingxiao Zheng,[a,b] Yani Liu,[a,b] Xinrui Zheng,[a,b] Yaqin Wang,[a,b] Wanying Han[a,b] and Buxing Han *[a,b,c,d]

Received 1st November 2023,
Accepted 19th February 2024

DOI: 10.1039/d3gc04217k

rsc.li/greenchem

Lignin is composed of phenylpropyl alcohol through the C–O and C–C bonds, where β-O-4 accounts for the majority. Self-transfer hydrogenolysis (STH) is a promising method to produce valuable chemicals and fuels from lignin by cleaving the β-O-4 bond without exogenous hydrogen, but all the reported work used noble metal-based catalysts. In this work, a highly efficient Ni/C catalyst was derived from a Ni-containing metal–organic framework (Ni-MOF), and its self-transfer hydrogenolysis performance towards ether bonds in lignin model compounds was evaluated using 2-phenoxy-1-phenylethanol as a model compound in detail. It was found that the catalyst pyrolyzed under a nitrogen atmosphere at 500 °C (Ni-NDC-500) was very efficient for the reaction. Moreover, it could also catalyze the reaction of native lignin into monomers effectively without exogenous hydrogen. In addition, Ni-NDC-500 was recycled three times without an obvious reduction of the activity.

1. Introduction

Due to the depletion of fossil resources, utilization of biomass as a sustainable, carbon-neutral supply of fuels and chemicals is an immediate need.[1–8] Lignocellulose is an important biomass, of which lignin is interesting due to its high aromatic content.[9] Lignin is a complex polymer connected by the C–O and C–C bonds.[10] The β-O-4 bonds, which occupy more than half of the linkage structure in lignin, are a main object of study. The cleavage of β-O-4 ether bonds of lignin compounds using hydrogen is usually referred to as hydrogenolysis.[11]

The liquid-phase hydrogenolysis reaction typically requires high H_2 pressures (1–20 MPa) to ensure better dissolution of H_2 into the reaction medium.[12] However, hydrogen cannot be naturally produced and is usually industrially produced by steam-reforming fossil fuels like coal, natural gas, and oil, leading to an increased carbon footprint during production and transportation. In addition to hydrogen gas, hydrogen donors are also utilized for the depolymerization and hydrogenolysis of lignin.[13] Lignin possesses abundant aliphatic hydroxyl groups capable of undergoing dehydrogenation (C_α–OH to C=O) to obtain hydrogen. Studies have shown that lignin can depolymerize into monomers without requiring additional hydrogen sources, utilizing the hydroxyl groups within lignin itself as the hydrogen donor. This approach is termed the self-hydrogen transfer hydrogenolysis (STH) process.[14] For the STH of lignin model compounds, Cai and coworkers used MIL-100(Fe) supported Pd–Ni bimetal nanoparticles.[15] The STH of native lignin to monomers over a Pd–PdO/TiO_2 catalyst was reported by Wang *et al.*[16]

In addition, the –OCH_3 group in lignin can provide a hydrogen source for the STH process through dehydrogenation or aqueous phase reforming. Wang's group used $NiAl_2O_4$ loading with various noble metals to produce alkylphenol from lignin by self-reforming-driven depolymerization and hydrogenolysis, and found that demethoxylation is the rate-determining step in the whole process.[17–19] Rong and Li reported the highly selective conversion of guaiacol to phenol in pure water by a versatile nano-porous Ni catalyst, and the mechanism showed that the initial hydrogen source came from water splitting on the surface of the Ni catalyst, and the subsequent aqueous phase reforming of methanol generated more hydrogen and further accelerated the hydrodeoxygenation process.[20] Our group proposed self-supported hydrogenolysis (SSH) of aromatic ethers to produce arenes using the methoxy group as the

[a]*Shanghai Key Laboratory of Green Chemistry and Chemical Processes, State Key Laboratory of Petroleum Molecular & Process Engineering, School of Chemistry and Molecular Engineering, East China Normal University, Shanghai 200062, China. E-mail: liuhz@iccas.ac.cn, hhwu@chem.ecnu.edu.cn, hanbx@iccas.ac.cn*
[b]*Institute of Eco-Chongming, Shanghai 202162, China*
[c]*School of Chemistry and Chemical Engineering, University of Chinese Academy of Sciences, Beijing 100049, China*
[d]*Beijing National Laboratory for Molecular Sciences, CAS Key Laboratory of Colloid and Interface and Thermodynamics, CAS Research/Education Center for Excellence in Molecular Sciences, Institute of Chemistry, Chinese Academy of Sciences, Beijing 100190, China*

†Electronic supplementary information (ESI) available: Materials, experimental procedure scheme of catalysts, lignin extraction process, synthesis of lignin model compounds, characterization of catalysts, GC profile, GC-MS data and NMR data. See DOI: https://doi.org/10.1039/d3gc04217k

hydrogen source over RuW/SiO_2.[21] The mechanism study showed that the aliphatic C–H bond in anisole was firstly activated and followed by the selective hydrogenolysis of C_{aryl}–OMe to generate benzene. And the RuW/HY_{30} catalyst could deconstruct the C_{sp_2}–C_{sp_3} and C_{sp_2}–O bonds in the lignin structure in an orderly manner, allowing the production of benzene exclusively from lignin.[22] These articles used water as the reaction medium, which is a cheap, non-toxic and environmentally friendly reaction medium.[15–22]

The reported works on the STH process are based on precious metal catalysts. However, the resources of precious metals are very limited, and mining and purification release large amounts of CO_2 compared with non-precious metals.[23] Therefore, it is highly promising to replace noble metals with abundant and inexpensive transition metals for the self-transfer hydrogenolysis and upgradation of lignin model compounds. Many research studies show that Ni-based catalysts could efficiently and selectively cleave the β-O-4 ether bonds of lignin.[24–26] MOF-derived catalysts prepared by controlled pyrolysis provide a route to synthesize catalysts containing high surface area and highly dispersed metal nanoparticles, which might facilitate the hydrogenolysis of lignin.[27] There have been many reports on MOF-derived catalysts for lignin hydrogenolysis, but the reaction was carried out under a hydrogen atmosphere.[28–30]

Herein, we report a simple method to obtain a Ni/C catalyst derived from Ni-MOF with high catalytic activity in the STH of lignin. The active sites and reaction mechanism of the catalysts were investigated in depth. This is the first work on inexpensive transition metals for the self-transfer hydrogenolysis process.

2. Experiment section

2.1 Catalyst preparation

Ni-MOF was prepared by the co-precipitation method reported in the literature.[31] Fig. S1† is a schematic of the preparation procedures of the Ni/C catalyst. $Ni(NO_3)_2{\cdot}6H_2O$ (4.06 g) and 1,4-naphthalenedicarboxylic acid (NDC, 2.94 g) were dissolved in *N*,*N*-dimethylformamide (DMF) (48 mL), ethanol (6 mL) and H_2O (6 mL). The mixture was mixed well using an ultrasonic process for 30 minutes, and then 12 mL of triethylamine was added to the mixture. After continuous ultrasound for four hours at room temperature, the precursors were collected by centrifugation and washed three times with ethanol and distilled water. The product was then dried overnight in a blast dryer at 120 °C. Ni-MOF (Ni-NDC) was obtained. Ni-NDC was then calcined in a tube furnace under nitrogen at 400, 500, 600 and 700 °C. The obtained catalysts are respectively denoted as Ni-NDC-400, Ni-NDC-500, Ni-NDC-600 and Ni-NDC-700.

2.2 Catalyst characterization

The phase and unit cell structures of synthesised catalysts were analyzed by powder XRD technique. XRD analysis was carried out on an XRD-Ultima IV diffractometer manufactured by Rigaku Corporation, Japan. The obtained XRD pattern was compared with a standard card to obtain the phase composition of the catalyst. X-ray photoelectron spectroscopy (XPS) was mainly used to analyze the surface element composition, valence charge and species of the catalyst. The K-Alpha type XPS produced by Thermo Fisher Company of the United States used an Al anode (energy of 1486.6 eV) as the excitation source and C 1s (284.6 eV binding energy) as the standard to calibrate the gas element. The morphology and particle size distributions of the catalysts were studied using HRTEM (FEI Tecnai F30). The N_2 adsorption–desorption method was used to analyze the specific surface areas of catalysts on a TriStar II Model 3020 adsorption desorber. The relevant specific surface area of the catalysts in this study was also obtained by the BET method on the instrument. Inductively coupled plasma atomic emission spectrometry (ICP-AES, Agilent Technologies, 5100) was adopted to measure the Ni content. The NMR spectra were acquired on a Bruker Avance II300 400 MHz spectrometer. The lignin sample was dissolved in deuterated dimethyl sulfoxide (DMSO-d_6). The central solvent peak at δ_C/δ_H 39.5/2.49 was used as an internal reference. Two-dimensional HSQC NMR experiments were used for structural characterization and assignment authentication. HSQC cross-peaks were assigned by combining the results and comparing them with the literature.

2.3 Catalyst activity tests

The catalytic reactions were conducted in a Teflon-lined stainless-steel autoclave (15 mL) with the desired dosages of the substrate, catalyst, internal standard (*n*-dodecane or *n*-hexadecane), and solvent. In a typical experiment, 64.2 mg (0.3 mmol) of 2-phenoxy-1-phenylethanol, 40 mg of Ni-NDC-500 catalyst, and 5 mL of distilled water were added to the reactor. The reactor was purged with N_2 three times to remove the air at room temperature. Then N_2 was charged to the desired pressure and the reactor was placed in a furnace at the desired temperature under an agitation speed of 800 rpm. After the reaction, the reactor was cooled down to room temperature and the gas was released. The liquid phase was carefully extracted with 2 mL of ethyl acetate. The qualitative analysis of reaction products was carried out on a GC-MS system (Agilent 7890A—5975C), and the quantitative analysis was executed on a GC system (Agilent 8890B) equipped with an HP-5 column and an FID detector.

3. Results and discussion

3.1 Characterization of catalysts

The crystallinity and crystalline phases of the prepared catalysts were investigated using X-ray diffraction. As shown in Fig. 1a, Ni-NDC exhibited a distinct characteristic peak at 7.9°, suggesting the successful synthesis of Ni-MOF.[31] The XRD pattern of Ni-NDC-400 revealed a mixed phase of NiO and Ni, suggesting incomplete reduction by carbon at a calcination

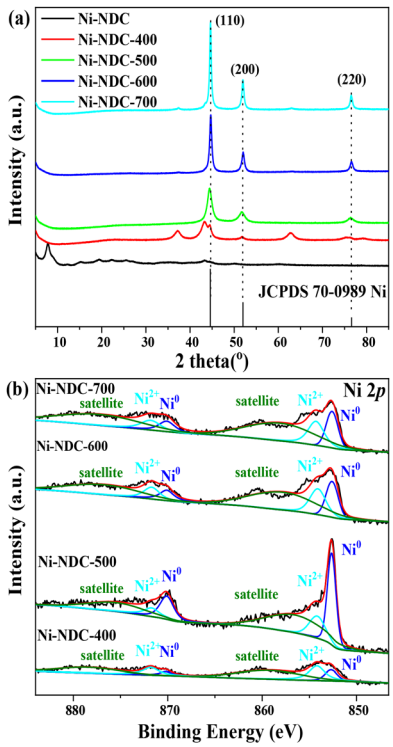

Fig. 1 XRD patterns (a) and XPS spectra (b) of the prepared catalysts.

temperature of 400 °C. The XRD patterns of Ni-NDC-500, Ni-NDC-600, and Ni-NDC-700 catalysts exhibited good agreement with the standard face-centred cubic structure of Ni^0 (JCPDS No. 70-0989), with diffraction peaks at 44.5°, 51.8°, and 76.3° corresponding to (111), (200), and (220) crystal planes, respectively. The findings suggested that the majority of Ni^{2+} ions in the Ni-NDC-500, Ni-NDC-600, and Ni-NDC-700 catalysts were reduced to Ni^0. Additionally, as the calcination temperature increased, the intensity of XRD peaks also increased, indicating larger crystalline grains and improved crystallinity.

XPS (X-ray photoelectron spectroscopy) was employed to examine the valence state of surface elements in the catalysts. Fig. 1b shows the Ni 2p XPS spectra of the calcined catalysts. The peaks observed at 870.1 eV and 852.6 eV correspond to Ni^0, while the peaks at 871.7 eV and 854.1 eV correspond to Ni^{2+}. Notably, Ni-NDC-500 exhibited the highest content of surface Ni^0.

The N_2 adsorption–desorption isotherms were used to determine the specific surface area and pore structure of the Ni-NDC catalysts. The results are presented in Fig. S2.† Ni-NDC exhibited a type II isotherm in the Brunauer classification and an obviously H3 hysteresis loop, which confirms its microporous characteristics. Notably, Ni-NDC-400 and Ni-NDC-500 also displayed a type II isotherm and H3 hysteresis loop, indicating the presence of a microporous structure. However, Ni-NDC-600 and Ni-NDC-700 exhibited an H4 hysteresis loop, indicating the presence of a mesoporous structure in the catalyst. The surface areas of the catalysts were calculated using the multi-point Brunauer–Emmett–Teller (BET) method, and the values are listed in Fig. S2.† The BET surface areas of Ni-NDC-400, Ni-NDC-500, Ni-NDC-600, and Ni-NDC-700 were 32.96, 122.19, 144.56, and 157.31 $m^2\ g^{-1}$, respectively. The significant specific surface area facilitated the substrate mass transfer and exposed catalytically active sites.

Table 1 presents the ICP results, and the Ni contents in Ni-NDC, Ni-NDC-400, Ni-NDC-500, Ni-NDC-600, and Ni-NDC-700 were 21.3%, 40.8%, 54.5%, 57.9%, and 60.5%, respectively. As the calcination temperature increased, the bulk Ni content also increased, indicating that a higher temperature resulted in carbon loss. Additionally, the lower surface Ni content observed through XPS suggests that a significant portion of Ni is encapsulated by carbon.

TEM and HR-TEM were employed to observe the morphology and spatial structure of the prepared catalysts. In Fig. 2a and b, the uncalcined catalyst did not exhibit any visible Ni metal particles. However, after calcination, uniformly dispersed Ni nanoparticles with an average size of approximately 10 nm were observed within the carbon framework (Fig. 2c–j). The HRTEM images revealed the detailed structure of these Ni nanoparticles, demonstrating high crystallinity and clear lattice fringes. The lattice spacings of 1.76 Å and 2.03 Å corresponded to the (200) plane and (111) plane of nickel, respectively, as per the JCPDS 70-0989 reference. These TEM observations aligned with the XRD results, showing that the average particle size of Ni increased gradually with the calcination temperature.[32]

Table 1 The conversion and yield of hydrogenolysis of 2-phenoxy-1-phenylethanol

Entry	Catalysts	Conv. (%)	Yield (%)					Bulk Ni[a] %	Surface Ni[b] %
			1b	1c	1d	1e	1f		
1	No catalysts	0	—	—	—	—	—	—	—
2	Ni-NDC	8.5	1.5	—	—	—	—	21.3	1.01
3	Ni-NDC-700	24.9	14.4	6.0	—	3.6	—	60.5	1.18
4	Ni-NDC-600	92.8	80.3	60.1	1.9	8.8	4.5	57.9	1.31
5	Ni-NDC-500	99.9	99.9	77.9	3.0	—	—	54.5	1.54
6	Ni-NDC-400	14.8	4.4	0.7	—	4.8	0.9	48.0	0.59

Reaction conditions: 40 mg catalysts, 0.3 mmol of 2-phenoxy-1-phenylethanol, 5 mL of distilled water, 220 °C, 2 h, initial pressure 2 MPa nitrogen, and stirring at 800 rpm. Yields and conversions were determined by GC relative to an internal standard. [a] Bulk Ni content was obtained by ICP-OES. [b] Surface Ni content was obtained by XPS.

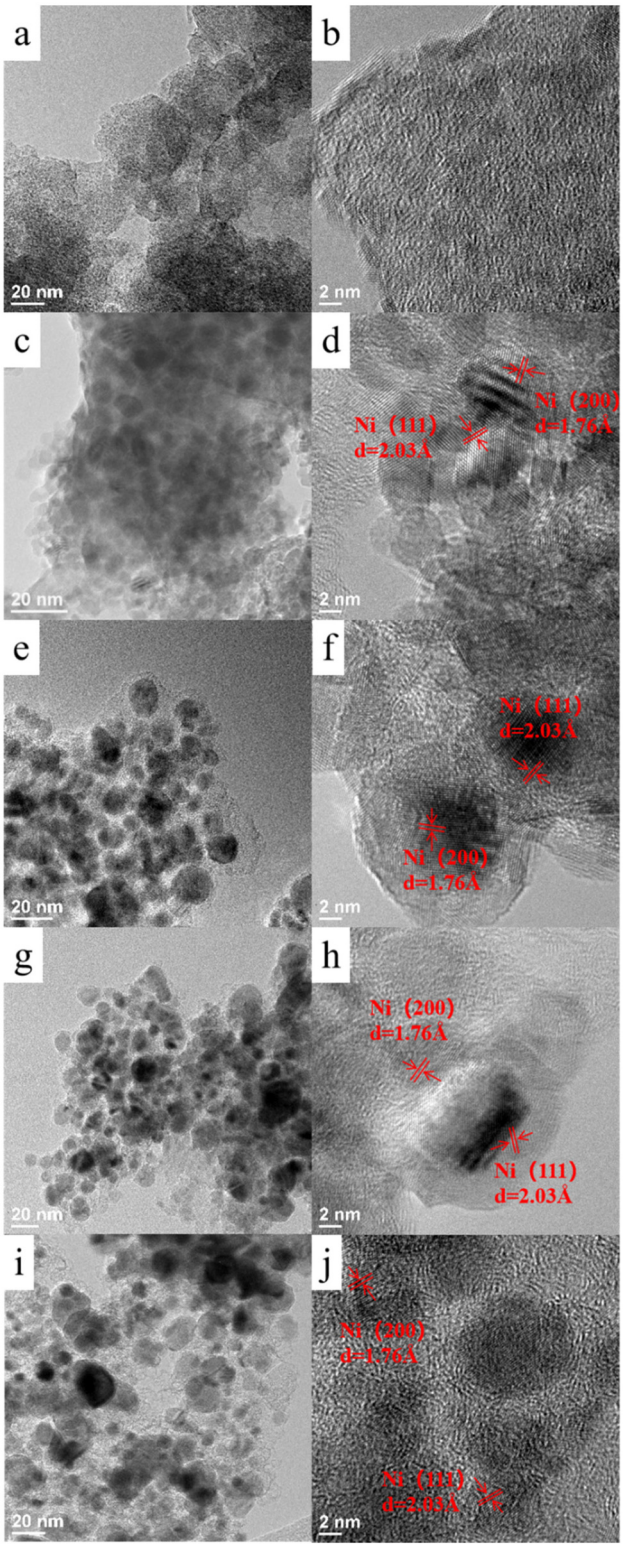

Fig. 2 TEM and HRTEM images of Ni-NDC (a and b), Ni-NDC-400 (c and d), Ni-NDC-500 (e and f), NDC-600 (g and h), and Ni-NDC-700 (i and j).

3.2 Effect of calcination temperature

2-Phenoxy-1-phenylethanol (**1a**) is a dimeric model compound of lignin and was used as a probe molecule to study the STH process of β-O-4 linkage. Phenol (**1b**), acetophenone (**1c**), ethylbenzene (**1d**), 2-phenoxyacetophenone (**1e**) and phenoxyethylbenzene (**1f**) were produced during the reaction process (Scheme 1). The performances of Ni-MOF and catalysts pyrolyzed at different temperatures are listed in Table 1. The substrate remains unconverted in the absence of a catalyst (Table 1, entry 1). However, upon adding catalysts, the conversions of **1a** significantly improved. The activity of Ni-NDC was very low and the conversion of **1a** was only 8.5% (Table 1, entry 2). Ni-NDC-400 also exhibited low activity due to the predominant presence of Ni^{2+} rather than active Ni^0 species. Ni-NDC-500 showed the best catalytic performance among the catalysts checked and the conversion of **1a** could reach 99.9% and the yields of phenol and acetophenone were 99.9% and 77.9%, respectively. A higher calcination temperature results in lower activity. Further increasing the calcination temperature led to decreased activity. Over Ni-NDC-600, the yields of phenol and acetophenone were 80.3% and 60.1%,

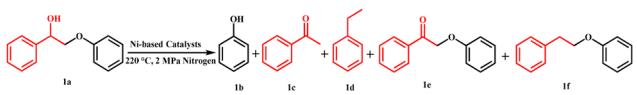

Scheme 1 Cleavage of 2-phenoxy-1-phenylethanol in the absence of external hydrogen over Ni-based catalysts.

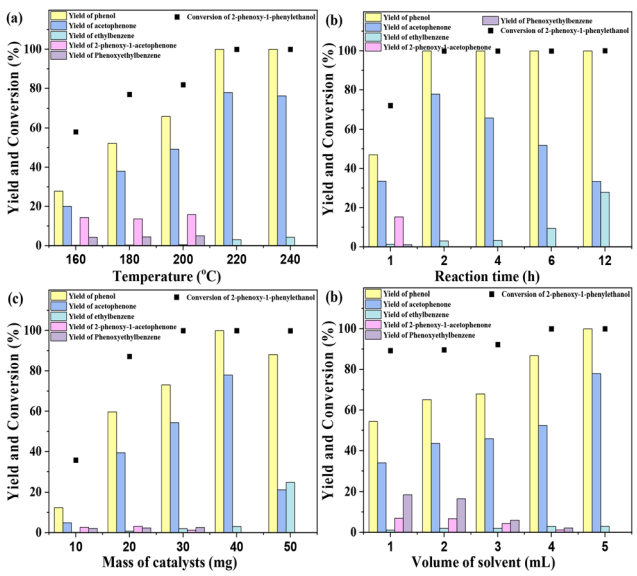

Fig. 3 The conversion and yield of hydrogenolysis of 2-phenoxy-1-phenylethanol over Ni-NDC-500 with (a) different temperature, (b) different reaction time, (c) different masses of catalysts and (d) different volumes of solvent. Reaction conditions: 40 mg of catalysts, 0.3 mmol of 2-phenoxy-1-phenylethanol, 5 mL of distilled water, 220 °C, 2 h, initial pressure 2 MPa nitrogen, and stirring at 800 rpm (unless otherwise specified). Yields and conversions were determined by GC relative to an internal standard.

respectively. However, these yields decreased significantly to 14.4% and 6.0% over Ni-NDC-700. The XRD, XPS, and TEM results indicated that excessively high temperatures caused Ni metal agglomeration and a decrease in Ni^0 content on the surface, while excessively low temperatures resulted in incomplete reduction of Ni to the metallic state. The optimal catalytic activity of Ni-NDC-500 could be attributed to its high surface Ni^0 content and the appropriate size of Ni nanoparticles.

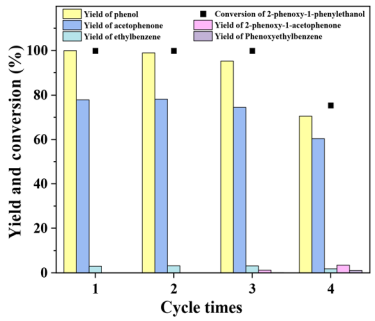

Fig. 4 Results for reuse of the catalyst in the conversion of 1-phenoxy-1-phenylethanol over Ni-NDC-500. Reaction conditions: 40 mg of catalysts, 0.3 mmol of substrate, 5 mL of distilled water, 220 °C, 2 h, initial pressure 2 MPa nitrogen, and stirring at 800 rpm. Yields and conversions were determined by GC relative to an internal standard.

3.3 Optimization of reaction conditions over Ni-NDC-500

The optimization of reaction conditions was performed using 2-phenoxy-1-phenylethanol as the probe molecule and Ni-NDC-500 as the catalyst. Initially, the impact of temperature on the STH reaction was investigated (Fig. 3a). Higher temperatures led to an increased conversion of **1a**, with a complete conversion at 220 °C. At this temperature, the yields of phenol and acetophenone were 99.9% and 77.9%, respectively. However, when the temperature rose to 240 °C, the yield of acetophenone decreased while the yield of ethylbenzene increased. The effect of reaction time was examined at 220 °C, as shown in Fig. 3b. With a reaction time of 2 h, the substrate was completely converted into acetophenone and phenol. Subsequently, as the reaction time extended, acetophenone underwent further hydrogenation to produce ethylbenzene. The reduction of acetophenone occurred through hydrogen derived from water, leading to the oxidation of the catalyst Ni^0 to Ni^{2+}. Additionally, Fig. 3c and d demonstrate the influence of solvent amount and catalyst quantity on the STH reaction.

Table 2 Hydrogenolysis of lignin models over the Ni-NDC-500 catalyst

Entry	Substrate	Conv. (%)	Yield of product (%)
1	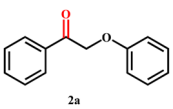 2a	99.9	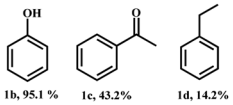 1b, 95.1 % 1c, 43.2% 1d, 14.2%
2	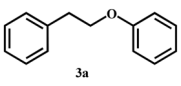 3a	75.3	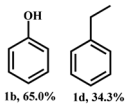 1b, 65.0% 1d, 34.3%
3	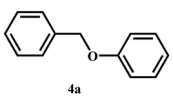 4a	99.9	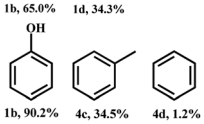 1b, 90.2% 4c, 34.5% 4d, 1.2%
4	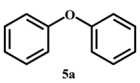 5a	7.0	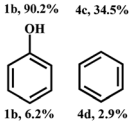 1b, 6.2% 4d, 2.9%
5	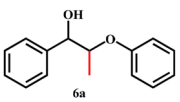 6a	90.5	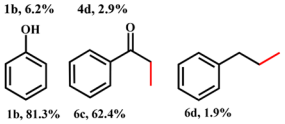 1b, 81.3% 6c, 62.4% 6d, 1.9%
6	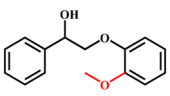 7a	81.4	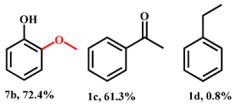 7b, 72.4% 1c, 61.3% 1d, 0.8%
7	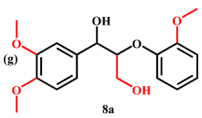 8a	75.2	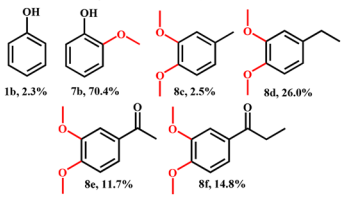 1b, 2.3% 7b, 70.4% 8c, 2.5% 8d, 26.0% 8e, 11.7% 8f, 14.8%

Reaction conditions: 40 mg of catalysts, 0.3 mmol of substrate, 5 mL of distilled water, 220 °C, 2 h, initial pressure 2 MPa nitrogen, and stirring at 800 rpm. Yields and conversions were determined by GC relative to an internal standard.

40 mg of the catalyst yielded relatively satisfactory results for the STH reaction. The amount of solvent also had a discernible effect on the reaction outcome, as an increase in solvent amount improved the reaction efficiency.

3.4 Reuse of the catalyst

The catalytic stability of the Ni-NDC-500 catalyst was assessed by conducting recycling experiments. The catalyst was recovered from the reaction mixture through magnetic separation (Fig. S3†), followed by washing and drying before being reused in the subsequent cycles. The performance of the catalyst did not change obviously over three cycles (Fig. 4). After four cycles, there was a slight decrease in reactivity. Comparison of the XPS spectra and XRD patterns (Fig. S4 and S5†) between the catalyst after four cycles and the fresh catalyst revealed no alterations in crystal structure. The surface $Ni^0/(Ni^0 + Ni^{2+})$ content decreased only from 71% to 57% after the four reaction cycles. Additionally, Fig. S6† shows the TEM image of the used catalyst, which closely resembles that of the original catalyst (Fig. 2e and f). These results further confirm that Ni-NDC-500 exhibits both a well-preserved spatial structure and robust catalytic stability during the STH reaction.

3.5 STH process of lignin models and native lignin

After establishing a reliable procedure, we investigated the substrate scope of the novel Ni-NDC-500-catalyzed hydrogenolysis reaction of lignin model compounds without external hydrogen. Notably, the catalyst effectively cleaved ether bonds in β-O-4 model substrates containing hydroxyl groups (**6a–8a**, Table 2, entries 5–7). Interestingly, it was also observed that the Ni-NDC-500 catalyst facilitated the cleavage of ether bonds in substrates lacking C_α–OH groups (**2a–5a**, Table 2, entries 1–4). This suggests that the catalyst could utilize hydrogen derived from H_2O to enable the cleavage of ether bonds. The X-ray diffraction (XRD) pattern in Fig. S7† demonstrates the emergence of NiO following the catalysis of the **2a** and **3a** transformations using Ni-NDC-500. This suggests that in the absence of Cα–OH in the substrate, hydrogen from water reduces the substrate, leading to the oxidation of Ni^0 to NiO.[20] Meanwhile 2-phenoxy-1-acetophenone (**2a**) exhibited lower reactivity compared to 2-phenoxy-1-phenylethanol (Scheme S1†), undergoing transformation into phenol and acetophenone using the Ni-NDC-500 catalyst, despite the lower ether bond energy in 2-phenoxy-1-acetophenone (**2a**, 227.8 kJ mol^{-1}) compared to 2-phenoxy-1-phenylethanol (**1a**, 274.0 kJ mol^{-1}).[33] This suggests that Ni-NDC-500 demonstrates higher activity for self-transfer hydrogenolysis using C_α–OH as the hydrogen source compared to transfer hydrogenolysis with H_2O as the hydrogen source, indicating that the STH process governs the reaction.

The self-transfer hydrogenolysis (STH) process of native lignin, extracted from poplar, eucalyptus, and sequoia wood powder using the Ni-NDC-500 catalyst, was carried out following established methods.[34] The obtained results, presented in Fig. 5 and Fig. S8,† revealed lignin monomer yields of 5.5%, 10.4%, and 7.4% by weight for poplar, eucalyptus, and metasequoia, respectively. Analysis conducted using 2D-HSQC and HMBC (Fig. S9–S11†) confirmed the efficient cleavage of β-O-4 bonds in lignin by the Ni-NDC-500 catalyst, with the resulting monomer retaining the methoxy group in the lignin unit structure.

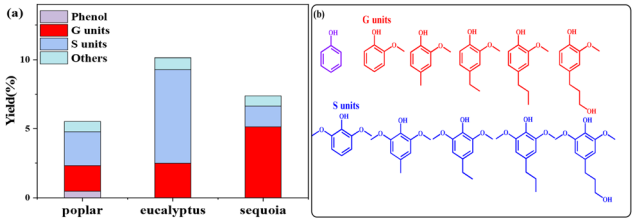

Fig. 5 Yield of lignin monomers (a) and the product distribution (b) from native lignin. Reaction conditions: 40 mg of Ni-NDC-500, 100 mg of lignin, 5 mL of distilled water, 240 °C, 12 h, initial pressure 2 MPa nitrogen, and stirring at 800 rpm. Yields of lignin monomers were determined by GC relative to an internal standard.

3.6 Main reaction pathway

Control experiments were conducted to investigate the reaction mechanism described in Scheme 2. When compound **1a** was transformed with Ni-NDC-500 at 150 °C for 12 hours, yields of 92.3% phenol (**1b**) and 63.6% acetophenone (**1c**) were obtained. However, no products were detected when (1-methoxy-2-phenoxyethyl)benzene (**9a**) was used under the same reaction conditions. These results highlight the impor-

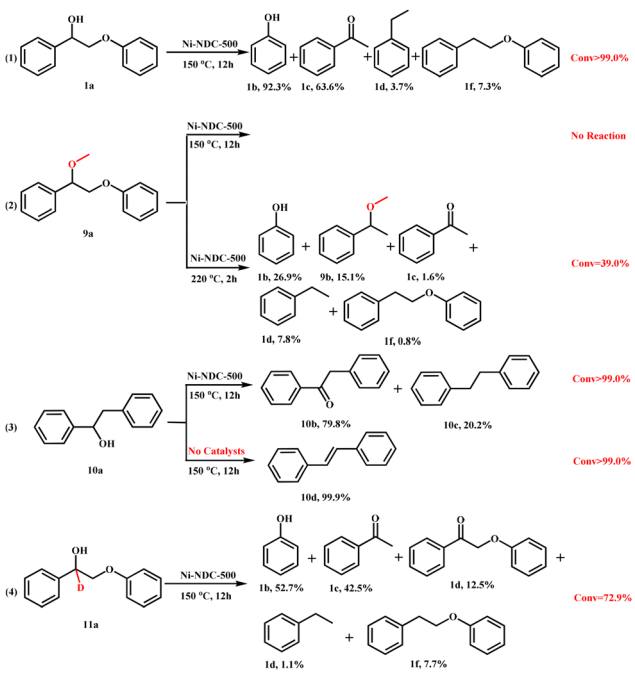

Scheme 2 Control experiments to study the reaction mechanism. Reaction conditions: 40 mg of catalysts, 0.3 mmol of substrate, 5 mL of distilled water, initial pressure 2 MPa nitrogen, and stirring at 800 rpm. Yields and conversions were determined by GC relative to an internal standard.

tance of C_α–OH groups in the transformation process. Interestingly, at 220 °C, (1-methoxy-2-phenoxyethyl)benzene (**9a**) exhibited 39% conversion, resulting in 26.9% phenol (**1b**), 15.1% (1-methoxyethyl)benzene (**9b**) and 7.8% ethylbenzene (**1d**). This suggests that the catalyst can facilitate ether bond cleavage by utilizing hydrogen derived from H_2O at 220 °C, while self-transfer hydrogenolysis utilizing C_α–OH as the hydrogen source process occurred at 150 °C. Furthermore, when 1,2-diphenylethanol (**10a**) was used as the substrate, the dehydration reaction took place and stilbene (**10d**) was produced in the absence of a catalyst, while the dehydrogenation reaction proceeded with Ni-NDC-500 and 1,2-diphenylethan-1-one (**10b**) was produced.

Based on the obtained results, a proposed pathway and the reaction mechanism are presented in Scheme 3. The reaction initiates with the dehydrogenation of 2-phenoxy-1-phenylethanol, resulting in the formation of 2-phenoxy-1-acetophenone and the adsorption of chemically bound hydrogen ("hydrogen pool") on Ni nanoparticles.[35,36] Subsequently, the presence of atomic hydrogen on Ni-NDC-500 facilitates the cleavage of the β-O-4 linkage to form acetophenone and phenol.

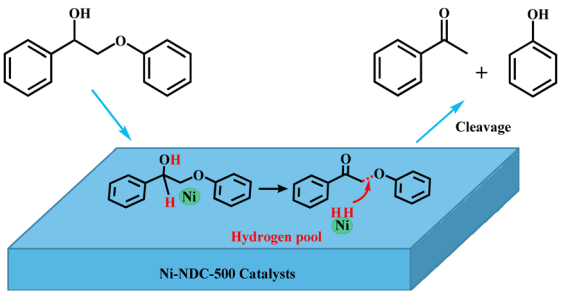

Scheme 3 Reaction mechanism of the lignin β-O-4 model cleavage to produce phenol and acetophenone over Ni-NDC-500 catalysts without external hydrogen.

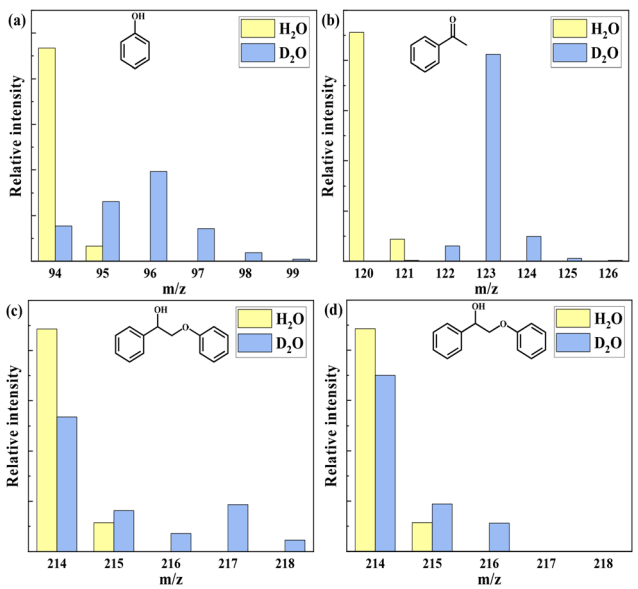

Fig. 6 The relative molecular mass of products determined in GC-MS after a 12 h reaction with catalysts (a–c) and without catalysts (d). Reaction conditions: 40 mg of catalysts, 0.3 mmol of 2-phenoxy-1-phenylethanol, 5 mL of solvent, 150 °C, 12 h, initial pressure 2 MPa nitrogen, and stirring at 800 rpm.

Isotopic labeling was used to further validate the reaction mechanism. When the C_α position of 2-phenoxy-1-phenylethanol is replaced by deuterium (**11a**), the reaction rate slows down due to the isotopic effect.[37] The reactions were performed in H_2O and D_2O. The mass spectrometry of **1a** and hydrogenolysis products shows deuterium labelled phenol and acetophenone under the reaction conditions. It is worth noting that deuterium labelled **1a** was also detected after 12 h at 150 °C even in the absence of catalyst (Fig. 6d, Fig. S12–S14†). The NMR data showed that an H/D exchange occurred between C_α–OH and D_2O and C_α–OH changed to C_α–OD even in the absence of catalyst (Fig. S15†). In the presence of catalyst, **1a** with a molecular weight of 218 was detected, implying that more H/D exchange of the substrate occurred in the presence of Ni.[38] A primary isotope effect was observed (the ratio of reaction rates using H_2O and D_2O, k_{H_2O}/k_{D_2O} = 1.51, Fig. S17†) at 150 °C, suggesting that the dehydrogenation (C_α–OH into C_α=O) is the rate-determining step.

4. Conclusions

Ni-MOF was used as a precursor to prepare the Ni/C catalyst, which could catalyze the transformation of lignin model compounds and lignin into monomers. The performance of the catalysts depended strongly on the calcination temperature, and the Ni-NDC-500 catalyst showed the best performance among the catalysts pyrolyzed at different temperatures, leading to an efficient cleavage of various lignin model compounds and native lignin into monomers with high yields. In addition, the catalyst was reused three times without obvious reduction in activity. Based on the findings from control experiments, possible reaction pathways have been proposed. The suggested reaction mechanism involves two steps: the dehydrogenation of C_α–OH on Ni-NDC-500 to generate a C_α=O intermediate and a "hydrogen pool", followed by the hydrogenolysis of the ether bond in the C_α=O intermediate facilitated by the "hydrogen pool". This study represents a novel work on the utilization of non-precious metal-based catalysts for the STH process of lignin.

Conflicts of interest

There are no conflicts to declare.

Acknowledgements

The authors thank the National Natural Science Foundation of China (22293012, 22179132, 22293015, and 22121002) and the Research Funds of Happiness Flower ECNU (2020ST2203) for support.

References

1 C. O. Tuck, E. Pérez, I. T. Horváth, R. A. Sheldon and M. Poliakoff, *Science*, 2012, **337**, 695–699.
2 G. Liu, A. W. Robertson, M. M. Li, W. C. H. Kuo, M. T. Darby, M. H. Muhieddine, Y. C. Lin, K. Suenaga, M. Stamatakis, J. H. Warner and S. C. E. Tsang, *Nat. Chem.*, 2017, **9**, 810–816.
3 B. Zheng, J. Song, H. Wu, S. Han, J. Zhai, K. Zhang, W. Wu, C. Xu, M. He and B. Han, *Green Chem.*, 2021, **23**, 268–273.
4 Y. Yang, Y. Wang, S. Li, X. Shen, B. Chen, H. Liu and B. Han, *Green Chem.*, 2020, **22**, 4937–4942.
5 S. Li, M. Dong, M. Peng, Q. Mei, Y. Wang, J. Yang, Y. Yang, B. Chen, S. Liu, D. Xiao, H. Liu, D. Ma and B. Han, *Innovation*, 2022, **3**, 100189.
6 Y. Liao, S.-F. Koelewijn, G. Van den Bossche, J. Van Aelst, S. Van den Bosch, T. Renders, K. Navare, T. Nicolaï, K. Van Aelst, M. Maesen, H. Matsushima, J. M. Thevelein, K. Van Acker, B. Lagrain, D. Verboekend and B. F. Sels, *Science*, 2020, **367**, 1385–1390.
7 Y. Queneau and B. Han, *Innovation*, 2022, **3**, 100184.
8 H. Liu, T. Jiang, B. Han, S. Liang and Y. Zhou, *Science*, 2009, **326**, 1250–1252.
9 M. Cao, B. Chen, T. Ruan, X. Ouyang and X. Qiu, *Acta Phys.-Chim. Sin.*, 2022, **38**(10), 2204037.
10 H. Zhou, Y. Jing and Y. Wang, *Acta Phys.-Chim. Sin.*, 2022, **38**(10), 2203016.
11 J. Zhang, *Green Energy Environ.*, 2018, **3**, 328–334.
12 A. Bjelić, M. Grilc, M. Huš and B. Likozar, *Chem. Eng. J.*, 2019, **359**, 305–320.
13 C. Espro, B. Gumina, T. Szumelda, E. Paone and F. Mauriello, *Catalysts*, 2018, **8**, 313.
14 J. M. Nichols, L. M. Bishop, R. G. Bergman and J. A. Ellman, *J. Am. Chem. Soc.*, 2010, **132**, 12554–12555.
15 J.-w. Zhang, G.-p. Lu and C. Cai, *Green Chem.*, 2017, **19**, 4538–4543.
16 Z. Dou, Z. Zhang and M. Wang, *Appl. Catal., B*, 2022, **301**, 120767.
17 L. Li, L. Dong, D. Li, Y. Guo, X. Liu and Y. Wang, *ACS Catal.*, 2020, **10**, 15197–15206.
18 L. Li, T. Zhang, Z. Guo, X. Liu, Y. Guo, Y. Huang and Y. Wang, *Ind. Eng. Chem. Res.*, 2021, **60**, 11699–11706.
19 Z. Guo, L. Li, Y. Guo, X. Liu and Y. Wang, *Catal. Sci. Technol.*, 2022, **12**, 5143–5151.
20 X. Ren, Z. Sun, J. Lu, J. Cheng, P. Zhou, X. Yu, Z. Rong and C. Li, *Green Chem.*, 2023, **25**, 1955–1969.
21 Q. Meng, J. Yan, H. Liu, C. Chen, S. Li, X. Shen, J. Song, L. Zheng and B. Han, *Sci. Adv.*, 2019, **5**, eaax6839.
22 Q. Meng, J. Yan, R. Wu, H. Liu, Y. Sun, N. Wu, J. Xiang, L. Zheng, J. Zhang and B. Han, *Nat. Commun.*, 2021, **12**, 4534.
23 X. Shen, C. Zhang, B. Han and F. Wang, *Chem. Soc. Rev.*, 2022, **51**, 1608–1628.
24 X. Shen, Y. Xin, H. Liu and B. Han, *ChemSusChem*, 2020, **13**, 4367–4381.
25 Q. Song, F. Wang, J. Cai, Y. Wang, J. Zhang, W. Yu and J. Xu, *Energy Environ. Sci.*, 2013, **6**, 994–1007.
26 H. Luo, I. M. Klein, Y. Jiang, H. Zhu, B. Liu, H. I. Kenttämaa and M. M. Abu-Omar, *ACS Sustainable Chem. Eng.*, 2016, **4**, 2316–2322.
27 A. Shivhare, D. Jampaiah, S. K. Bhargava, A. F. Lee, R. Srivastava and K. Wilson, *ACS Sustainable Chem. Eng.*, 2021, **9**, 3379–3407.
28 Q. Wang, L.-P. Xiao, Y.-H. Lv, W.-Z. Yin, C.-J. Hou and R.-C. Sun, *ACS Catal.*, 2022, **12**, 11899–11909.
29 X.-G. Si, Y.-P. Zhao, Q.-L. Song, J.-P. Cao, R.-Y. Wang and X.-Y. Wei, *React. Chem. Eng.*, 2020, **5**, 886–895.
30 W. Wu, H. Liu, H. Wu, B. Zheng, S. Han, K. Zhang, X. Mei, C. Xu, M. He and B. Han, *ACS Sustainable Chem. Eng.*, 2021, **9**, 11862–11871.
31 M.-Y. Zong, C.-Z. Fan, X.-F. Yang and D.-H. Wang, *Mol. Catal.*, 2021, **509**, 111609.
32 Y. Guo, X. Gao, C. Zhang, Y. Wu, X. Chang, T. Wang, X. Zheng, A. Du, B. Wang, J. Zheng, K. Ostrikov and X. Li, *J. Mater. Chem. A*, 2019, **7**, 8129–8135.
33 C. Zhang, J. Lu, X. Zhang, K. MacArthur, M. Heggen, H. Li and F. Wang, *Green Chem.*, 2016, **18**, 6545–6555.
34 L. Dong, L. Lin, X. Han, X. Si, X. Liu, Y. Guo, F. Lu, S. Rudić, S. F. Parker, S. Yang and Y. Wang, *Chem*, 2019, **5**, 1521–1536.
35 M. V. Galkin, C. Dahlstrand and J. S. Samec, *ChemSusChem*, 2015, **8**, 2187–2192.
36 N. Luo, M. Wang, H. Li, J. Zhang, T. Hou, H. Chen, X. Zhang, J. Lu and F. Wang, *ACS Catal.*, 2017, **7**, 4571–4580.
37 X. Zhao, J. Wang, L. Lian, G. Zhang, P. An, K. Zeng, H. He, T. Yuan, J. Huang, L. Wang and Y.-N. Liu, *ACS Catal.*, 2023, **13**, 2326–2334.
38 M. Gómez-Gallego and M. A. Sierra, *Chem. Rev.*, 2011, **111**, 4857–4963.